

Revisiting Unknowns: Towards Effective and Efficient Open-Set Active Learning

Chen-Chen Zong, Yu-Qi Chi, Xie-Yang Wang, Yan Cui, Sheng-Jun Huang*
 Nanjing University of Aeronautics and Astronautics
 Nanjing, 211106, China

{chencz, chiyuqi, xieyang, cuiyan, huangsj}@nuaa.edu.cn

Abstract

Open-set active learning (OSAL) aims to identify informative samples for annotation when unlabeled data may contain previously unseen classes—a common challenge in safety-critical and open-world scenarios. Existing approaches typically rely on separately trained open-set detectors, introducing substantial training overhead and overlooking the supervisory value of labeled unknowns¹ for improving known-class learning. In this paper, we propose E²OAL (Effective and Efficient Open-set Active Learning), a unified and detector-free framework that fully exploits labeled unknowns for both stronger supervision and more reliable querying. E²OAL first uncovers the latent class structure of unknowns through label-guided clustering in a frozen contrastively pre-trained feature space, optimized by a structure-aware F1-product objective. To leverage labeled unknowns, it employs a Dirichlet-calibrated auxiliary head that jointly models known and unknown categories, improving both confidence calibration and known-class discrimination. Building on this, a logit-margin purity score estimates the likelihood of known classes to construct a high-purity candidate pool, while an OSAL-specific informativeness metric prioritizes partially ambiguous yet reliable samples. These components together form a flexible two-stage query strategy with adaptive precision control and minimal hyperparameter sensitivity. Extensive experiments across multiple OSAL benchmarks demonstrate that E²OAL consistently surpasses state-of-the-art methods in accuracy, efficiency, and query precision, highlighting its effectiveness and practicality for real-world applications. The code is available at github.com/chenchenzong/E2OAL.

1. Introduction

Deep learning has achieved remarkable success across a wide range of domains, largely fueled by the availability

of large-scale datasets with high-quality annotations [9, 16, 25]. However, collecting such annotations is often prohibitively expensive, requiring extensive human effort and domain expertise [26, 30]. These limitations hinder the deployment of deep models in real-world scenarios where labeled data is scarce or costly.

Active learning (AL) mitigates this issue by iteratively selecting a small yet informative subset for annotation [30]. Traditional AL methods typically select samples based on model uncertainty [31, 37, 40], sample diversity [1, 28, 36], or combinations thereof [13, 22, 32]. Despite their success, most AL methods assume a *closed set*—that all unlabeled samples belong to known classes [20]. This assumption rarely holds in practice, especially in safety-critical domains such as autonomous driving [23, 35] or medical diagnosis [4, 33], where unlabeled data often includes samples from previously unseen classes. Under such open-set conditions, conventional AL strategies tend to over-select unknown class samples—mistaking their high uncertainty or feature-level novelty for informativeness—thereby degrading the overall learning process. These challenges motivate the study of open-set active learning (OSAL), which aims to query informative yet class-consistent samples while properly handling unknowns.

Recent advances in OSAL incorporate surrogate out-of-distribution (OOD) detection mechanisms to guide querying [6, 20, 21, 27, 38, 41, 42]. These methods typically combine uncertainty or diversity with auxiliary OOD scores to balance informativeness and purity. However, they often rely on separately trained OOD detectors, which incur substantial training overhead, and further overlook the potential of labeled unknowns as valuable supervision for enhancing known-class learning. This observation calls for a unified, detector-free OSAL framework that can both detect and utilize unknowns to enhance learning and querying.

To explore this, we first conduct a pilot study examining whether labeled unknowns benefit known-class learning. Assuming access to ground-truth labels for labeled unknowns, we train a dual-head classifier: a primary head optimized for known classes and an auxiliary head

*Corresponding Author.

¹Here, unknowns denotes samples from unknown (open-set) classes.

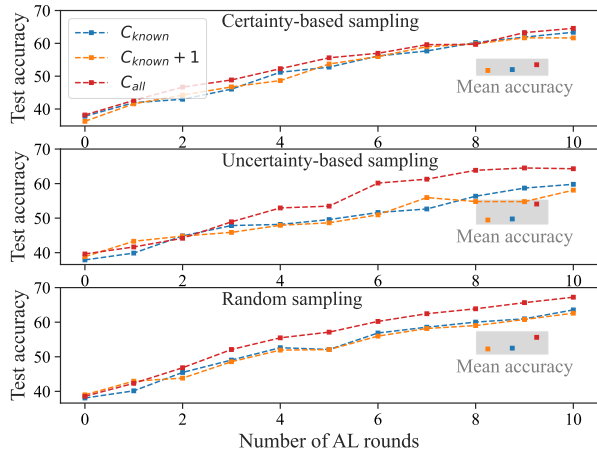


Figure 1. Per-round and mean test accuracy on CIFAR-100 (40 known / 60 unknown) using ResNet-18. C_{known} excludes labeled unknowns, $C_{known+1}$ collapses them into a single “unknown” class, and C_{all} leverages their true labels. C_{all} consistently performs best, suggesting that preserving the latent structure of unknown classes benefits known-class learning.

jointly trained on both known and unknown categories. As shown in Figures 1 and C1 (Appendix), incorporating labeled unknowns into training with their ground-truth labels consistently improves test accuracy. In contrast, merging them into a single “unknown” class may hinder performance. These results reveal that the latent structure within unknowns provides useful inductive signals. Meanwhile, a well-designed auxiliary head can also implicitly support unknowns detection—without explicit OOD models.

In this paper, we present E²OAL (Effective and Efficient Open-set Active Learning), a unified, detector-free OSAL framework that converts unknown-class feedback into both stronger supervision and more informative queries. At each AL round, E²OAL estimates the number and composition of unknown classes by clustering all labeled samples, including both knowns and unknowns, in a frozen contrastively representation space. The optimal cluster count is determined by aligning clusters with known labels and maximizing a structure-aware F1-product objective. To leverage supervision from labeled unknowns, E²OAL employs a Dirichlet-calibrated auxiliary head that improves known-class discrimination and provides calibrated confidence under open-set conditions. For query selection, we introduce a lightweight logit-margin purity score to estimate the likelihood of known classes and a tailored informativeness metric that favors samples with moderate uncertainty while suppressing those with overly ambiguous or confident predictions. These scores drive a two-stage query strategy: first constructing a high-purity candidate pool, then selecting the most informative samples for annotation. Crucially, the candidate pool size is dynamically adjusted to meet a tar-

get query precision, without introducing additional hyperparameters. Our main contributions are summarized as:

- We propose E²OAL, a unified and detector-free OSAL framework that transforms unknown-class feedback into both effective supervision and informative querying.
- We introduce a label-guided clustering strategy for automatic class estimation within a contrastive feature space, enabling structure-aware discovery of unknown classes.
- We develop a Dirichlet-calibrated auxiliary head with an associated logit-margin purity score to enhance known-class learning and provide reliable confidence calibration.
- We design an OSAL-specific informativeness metric that favors samples with moderate uncertainty while suppressing overly ambiguous or overconfident ones.
- We present a flexible two-stage selection scheme that dynamically adjusts to maintain a fixed target query precision—without introducing additional hyperparameters.
- Extensive experiments on multiple OSAL benchmarks show that E²OAL consistently outperforms state-of-the-art methods in accuracy, efficiency, and query precision.

2. Related Work

Active learning (AL) aims to reduce annotation cost by selectively querying the most informative samples while maintaining model performance [26, 30]. Classical AL approaches can be broadly categorized into uncertainty-based, diversity-based, and hybrid strategies. Uncertainty-based methods query samples with high model uncertainty, measured by entropy [12], margin [3], confidence scores [18], or Monte Carlo dropout variance [7]. Diversity-based methods instead seek to represent the underlying data distribution through clustering [19] or coresets selection [28]. Hybrid methods, such as BADGE [2], combine both uncertainty and diversity by clustering in the gradient space to balance representativeness and informativeness.

Most conventional AL methods operate under a closed-set assumption, where unlabeled and labeled data share the same label space. This assumption, however, fails in open-set active learning (OSAL), where the unlabeled pool may contain out-of-distribution (OOD) or open-set samples irrelevant to the known classes. In such cases, standard AL strategies often over-select OOD samples that appear uncertain or diverse yet provide little learning value—much like requesting annotations for unrelated concepts—ultimately degrading model performance.

To address this, various OSAL methods have been developed. LfOSA [20] trains an auxiliary detector to distinguish known classes, guiding queries using maximum activation values. MQNet [21] adopts a meta-learning framework that balances purity and informativeness via a multi-layer perceptron. More recent works such as EOAL [27], BUAL [42], and EAOA [41] jointly assess purity and informativeness within a detector-based paradigm: EOAL

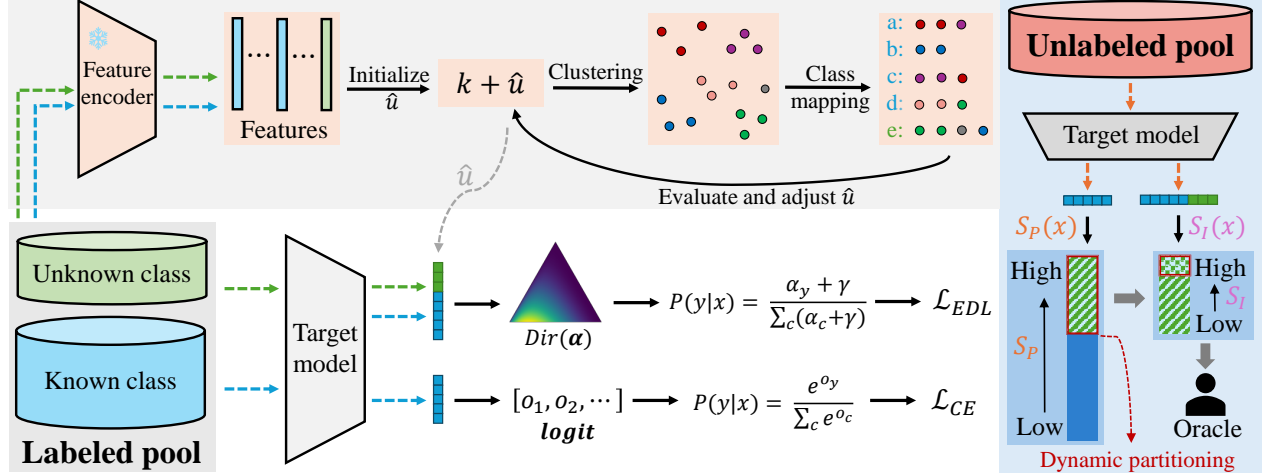


Figure 2. Overview of the proposed E²OAL framework. Each AL round consists of two stages: (1) Adaptive class estimation and calibration-aware training, where latent unknown classes are discovered via label-guided clustering and incorporated into model learning through Dirichlet-based auxiliary supervision; (2) Flexible two-stage query selection, where a high-purity candidate pool is first constructed using a purity score guided by a target query precision, followed by informativeness-driven sample selection.

defines separate entropy scores for known and unknown classes; BUAL leverages bidirectional uncertainty to refine selection boundaries; and EAOA integrates epistemic and aleatoric uncertainty for improved sample evaluation.

Despite recent progress, most OSAL methods still depend on separately trained detector networks, which add notable computational burden. In addition, they fail to fully exploit labeled unknowns—annotations that could provide valuable supervision for improving known-class discrimination. These limitations motivate our work, which revisits the role of labeled unknowns and introduces a unified, detector-free OSAL framework that converts them into effective supervision and reliable query guidance.

3. The Proposed Approach

In this section, we present E²OAL, a unified and detector-free framework for open-set active learning (OSAL) in multi-class image classification, where the unlabeled pool may contain samples from previously unseen classes. An overview of the framework is illustrated in Figure 2, with detailed pseudocode provided in Algorithm B1 (Appendix).

3.1. Preliminaries

Notations. We consider an OSAL setting where the unlabeled pool \mathcal{D}_U contains both known and unknown classes. Let \mathcal{C}_k and \mathcal{C}_u denote the sets of known and unknown classes, with $|\mathcal{C}_k| = k$, $|\mathcal{C}_u| = u$, and $\mathcal{C}_k \cap \mathcal{C}_u = \emptyset$. The labeled set \mathcal{D}_L initially includes only samples from \mathcal{C}_k , while \mathcal{D}_U covers $\mathcal{C}_k \cup \mathcal{C}_u$, with $|\mathcal{D}_L| \ll |\mathcal{D}_U|$. At each active learning (AL) round, a batch $\mathcal{B} \subset \mathcal{D}_U$ is queried and annotated. If a sample belongs to \mathcal{C}_k , its true class label is provided; otherwise, it receives a single “unknown” label,

without revealing its actual class in \mathcal{C}_u . The newly labeled batch is added to \mathcal{D}_L , resulting in $\mathcal{D}_L = \mathcal{D}_L^{kno} \cup \mathcal{D}_L^{unk}$ for known and unknown subsets, respectively. The observed query precision is $\bar{p}^* = |\mathcal{B}^{kno}|/|\mathcal{B}|$. Our goal is to train a classifier f_θ that generalizes well on \mathcal{C}_k with minimal labeling cost, even under contamination from unknowns.

Overview. Each AL round in E²OAL proceeds in two sequential stages: first, it uncovers and exploits the latent class structure of labeled unknowns to strengthen model training; then, it selects informative yet likely-known instances through an adaptive query strategy.

In stage 1, E²OAL performs label-guided clustering on \mathcal{D}_L within a frozen contrastive representation space (e.g., from CLIP [25], MoCo [10], or SimCLR [5]) to reveal latent unknown-class structures. A simple structure-aware F1-product objective determines the optimal cluster configuration, enabling adaptive class discovery. The resulting pseudo-clusters are treated as auxiliary classes for an additional classification head, trained jointly with the primary head using a Dirichlet-based calibration loss. This joint training improves known-class discrimination and yields calibrated confidence estimates. *In stage 2*, E²OAL estimates a logit-margin purity score for each unlabeled sample to measure its likelihood of belonging to known classes. Samples surpassing an adaptively adjusted purity margin, set to maintain a target query precision, form a high-purity candidate pool. Within this pool, a tailored informativeness metric evaluates each sample’s utility under open-set uncertainty, prioritizing those that are both reliable and informative. By combining these mechanisms, E²OAL adaptively selects high-quality queries and achieves efficient, detector-free OSAL without additional hyperparameter tuning.

3.2. Adaptive Class Estimation

To utilize labeled `unknowns` effectively, E²OAL estimates the latent class structure of \mathcal{D}_L^{unk} , including both the number and composition of unknown categories. Unlike traditional clustering methods that assume a fixed number of classes, E²OAL operates under the open-set assumption, where neither the number nor the granularity of unknown classes is known a priori.

To capture latent relationships among samples, we operate in a semantically rich and noise-robust contrastively pretrained feature space. Here, we leverage frozen representations from CLIP [25]², a pre-trained vision-language model known for providing high-quality, task-agnostic embeddings without additional fine-tuning. Within this feature space, we perform clustering on the labeled set \mathcal{D}_L . For each candidate number of clusters $\hat{u} \in \{k + 1, k + 2, \dots, \hat{u}_{max}\}$, clustering quality is evaluated by one-to-one aligning predicted assignments with ground-truth labels (covering k known classes and a unified “unknown” class) using Hungarian algorithm [15]. Assignments unmatched to known classes are treated as unknown categories. The clustering score is defined as the product of per-class F1 scores, jointly capturing alignment and structural fidelity.

The choice of \hat{u} has a strong impact on clustering quality [34]: underestimating \hat{u} may merge distinct known classes, while overestimating it can fragment coherent ones; both reduce the F1 score and hence the product. To determine the optimal \hat{u} efficiently, we employ a ternary search to maximize the F1-product score, thereby identifying the best cluster configuration. Each labeled unknown sample is then assigned to its nearest inferred cluster, which serves as a proxy category for downstream training.

The detailed pseudocode is provided in Algorithm 1.

3.3. Dirichlet-Based Calibration

While incorporating labeled `unknowns` improves generalization, reliable confidence estimation in open-set settings remains challenging. Standard softmax classifiers are notoriously overconfident [8, 29, 43], especially for outliers, because the softmax function is translation-invariant—adding or subtracting a constant from all logits does not alter the predicted probabilities. For example, logits $[0, 5, 0, 0]$ and $[-5, 0, -5, -5]$ both yield a softmax confidence of roughly 0.88 for the second class, even though the latter encodes far weaker semantic evidence. This results in misleadingly high confidence for semantically ambiguous or abnormal inputs, which is particularly detrimental in OSAL, where confidence estimation plays a critical role.

To alleviate this overconfidence, we adopt a translation-aware variant of softmax that explicitly breaks translation

²Our experiments show that MoCo and CLIP achieve similar performance, while CLIP can be directly used without additional training.

Algorithm 1 The adaptive class estimation algorithm

Input: Labeled data pool $\mathcal{D}_L = \{(x_i, y_i)\}$, known class count k , and upper limit \hat{u}_{max}

Output: Estimated number of unknown classes \hat{u}

- 1: Extract CLIP features $\{f_i\}$ for all $x_i \in \mathcal{D}_L$
- 2: # Ternary search for optimal unknown class count
- 3: Initialize bounds: $l \leftarrow k + 1, r \leftarrow \hat{u}_{max}$
- 4: **while** $r - l > 2$ **do**
- 5: $m_1 \leftarrow \lfloor l + \frac{r-l}{3} \rfloor, m_2 \leftarrow \lfloor r - \frac{r-l}{3} \rfloor$
- 6: $s_{m_1} \leftarrow \text{EVALUATE}(m_1, \{f_i\}, k)$
- 7: $s_{m_2} \leftarrow \text{EVALUATE}(m_2, \{f_i\}, k)$
- 8: **if** $s_{m_1} < s_{m_2}$ **then**
- 9: $l \leftarrow m_1$
- 10: **else**
- 11: $r \leftarrow m_2$
- 12: **end if**
- 13: **end while**
- 14: $\hat{u} \leftarrow \arg \max_{m \in \{l, l+1, \dots, r\}} \text{EVALUATE}(m, \{f_i\}, k)$

Function $\text{EVALUATE}(m, \{f_i\}, k)$:

- 1: $C \leftarrow k + m$
 - 2: Perform K-Means clustering on $\{f_i\}$ into C clusters
 - 3: Match the $k + 1$ clusters to $k + 1$ classes—including all k known classes and a unified unknown class—using the Hungarian algorithm [15]
 - 4: Assign the remaining $(C - (k + 1))$ clusters to the unknown class as well
 - 5: Compute class-wise F1 scores $\{F1_c\}_{c=1}^{k+1}$
 - 6: **return** $\prod_{c=1}^{k+1} F1_c$
-

invariance by introducing an additive constant. Given logits $\mathbf{o} = [o_1, o_2, \dots, o_{k+\hat{u}}]$ for a sample x , the calibrated probability for class y is:

$$P(y|x) = \frac{e^{o_y} + \gamma}{\sum_{c=1}^{k+\hat{u}} (e^{o_c} + \gamma)}, \quad (1)$$

where $\gamma > 0$ is a calibration constant. This modification ensures that predicted probabilities reflect both relative logit magnitudes and absolute evidence. The additive term γ serves as a smoothing factor, suppressing overconfidence for low-evidence samples. For instance, with $\gamma = 1$, the probabilities for the above logits decrease from 0.88 to approximately 0.60 and 0.38, respectively, improving confidence separation between confident and ambiguous cases.

However, directly optimizing this formulation with the commonly adopted cross-entropy (CE) loss introduces a gradient mismatch: the additive constant enlarges the logit margin required for confident predictions, thereby requiring gradient compensation to maintain effective optimization.

A straightforward remedy is to impose auxiliary regularization (e.g., ℓ_2 or KL divergence) to promote calibrated outputs. However, such rigid constraints often conflict with

CE loss, leading to unstable optimization. To address this, we adopt Evidential Deep Learning (EDL) [17, 29, 43], which models predictive probabilities as Dirichlet distributions and provides a principled, soft calibration mechanism naturally aligned with the modified softmax.

In EDL, the predictive distribution $\mathbf{p} = [p_1, \dots, p_{k+\hat{u}}]$ is drawn from a Dirichlet distribution $\text{Dir}(\boldsymbol{\alpha})$, parameterized by $\boldsymbol{\alpha} = [\alpha_1, \dots, \alpha_{k+\hat{u}}]$. The expected class probability is:

$$P(y|x) = \mathbb{E}_{\mathbf{p} \sim \text{Dir}(\boldsymbol{\alpha})}[p_y] = \frac{\alpha_y}{\sum_{c=1}^{k+\hat{u}} \alpha_c}. \quad (2)$$

We define $\boldsymbol{\alpha}$ via the model’s logits as $\boldsymbol{\alpha} = \frac{g(\mathbf{o})}{\gamma} + \mathbf{1}$, where $g(\cdot)$ is a non-negative activation (e.g., exponential) and γ is the calibration constant in Eq. (1), which can be implicitly learned by the network during training. The term $e = g(\mathbf{o})$ represents the *evidence*—the model’s support for each class. Substituting $\boldsymbol{\alpha} = \frac{g(\mathbf{o})}{\gamma} + \mathbf{1}$ into Eq. (2) with $g(\cdot) = \exp(\cdot)$ recovers the translation-aware softmax in Eq. (1).

Training is guided by a composite objective combining predictive accuracy and distributional regularization. The first term, a negative log-likelihood (NLL) loss, encourages high expected confidence on the true label:

$$\mathcal{L}_{\text{NLL}} = -\log P(y|x) = -\log \frac{\alpha_y}{\sum_{c=1}^{k+\hat{u}} \alpha_c}. \quad (3)$$

The second term, a KL divergence, penalizes excessive evidence for incorrect classes by regularizing the output Dirichlet toward a non-informative uniform prior:

$$\mathcal{L}_{\text{KL}} = \text{KL}(\text{Dir}(\tilde{\boldsymbol{\alpha}}) \parallel \text{Dir}(\mathbf{1})), \quad (4)$$

where $\tilde{\boldsymbol{\alpha}} = \mathbf{y} + (1 - \mathbf{y}) \odot \boldsymbol{\alpha}$, \mathbf{y} is the one-hot label encoding, $\mathbf{1}$ is a vector of ones, and \odot denotes element-wise multiplication. The full expansion of Eq. (4) is provided in the Appendix (Sec. A).

Finally, the overall training loss is defined as:

$$\mathcal{L} = \mathcal{L}_{\text{CE}} + \mathcal{L}_{\text{EDL}} = \mathcal{L}_{\text{CE}} + (\mathcal{L}_{\text{NLL}} + \mathcal{L}_{\text{KL}}), \quad (5)$$

where the auxiliary head is optimized over $k + \hat{u}$ categories using \mathcal{L}_{NLL} and \mathcal{L}_{KL} , while the primary head only focuses on the known classes via \mathcal{L}_{CE} .

3.4. Flexible Information-Purity Sampling

E²OAL performs query selection by jointly balancing two key factors: class purity and sample informativeness. High informativeness promotes label efficiency, while high purity ensures that most queries originate from known classes, thereby minimizing contamination from unknowns.

A fundamental challenge in OSAL is to identify unlabeled samples that are most likely to belong to known classes. We address this by introducing a lightweight logit-margin purity score computed from the auxiliary head’s

calibrated logits. Under Dirichlet-based calibration, each logit encodes class-specific evidence: positive values indicate support, with larger magnitudes reflecting higher confidence, while negative values indicate rejection. For an unlabeled sample $x \in \mathcal{D}_U$, let $o_{(1)}$ and $o_{(2)}$ denote the highest logits among known and unknown classes, respectively. The purity score is defined as:

$$S_{\text{purity}}(x) = o_{(1)} - o_{(2)} = \max_{c \in \mathcal{C}_k} o_c - \max_{c \in \mathcal{C}_{\hat{u}}} o_c. \quad (6)$$

A higher $S_{\text{purity}}(x)$ indicates stronger evidence for known-class membership. Unlike softmax-based confidence margins, this metric explicitly measures evidence separation, providing enhanced robustness under open-set conditions.

E²OAL further prioritizes samples that are both likely from known classes and highly informative. To quantify informativeness under open-set conditions, we propose a Jensen–Shannon (JS) divergence–based metric between the primary head’s output and two reference distributions:

$$S_{\text{info}}(x) = \text{JS}(\mathbf{p} \parallel \mathbf{u}) \cdot \text{JS}(\mathbf{p} \parallel \mathbf{p}^{\text{max}}), \quad (7)$$

where \mathbf{p} is the predicted probability vector from the primary head, \mathbf{u} is the uniform distribution, and \mathbf{p}^{max} is the one-hot encoding of the most confident class in \mathbf{p} . This formulation emphasizes moderately uncertain samples, which diverge from both uniform and peaked distributions, thus favoring ambiguous yet informative instances while avoiding outliers or trivial predictions.

E²OAL integrates the above two metrics into a flexible two-stage selection scheme calibrated to meet a fixed target query precision p^* . *In stage 1*, a high-purity candidate pool $\mathcal{C}_{\text{pool}}$ is constructed by fitting a three-component Gaussian Mixture Model (GMM) [24] to all $S_{\text{purity}}(x)$ values in \mathcal{D}_U . Each GMM component corresponds to a distinct purity regime: high (known-class-like), low (unknown-class-like), and intermediate (ambiguous). Samples are ranked by their posterior probability of belonging to the high-purity component, and $\mathcal{C}_{\text{pool}}$ is expanded until the mean posterior probability of its bottom- $|\mathcal{B}|$ entries matches a calibrated query precision \hat{p}^* . Notably, due to systematic estimation bias, we use a calibrated query precision \hat{p}^* instead of directly applying the target precision p^* . To compensate for such systematic shifts, the calibrated precision \hat{p}^* is adaptively updated using the observed precision \bar{p}^* from the previous round and the target precision p^* as follows:

$$\hat{p}_{t+1}^* = \begin{cases} \max(p^*, \min(\hat{p}_t^* + (p^* - \bar{p}_t^*), 0), 1) & \text{if } t > 0, \\ p^* & \text{if } t = 0. \end{cases} \quad (8)$$

This adaptive mechanism eliminates manual threshold tuning and ensures stable query precision across rounds.

In stage 2, the top- $|\mathcal{B}|$ samples from $\mathcal{C}_{\text{pool}}$ are selected according to $S_{\text{info}}(x)$. This two-stage strategy achieves a principled balance between uncertainty-driven exploration and label-purity control, enabling robust and adaptive querying.

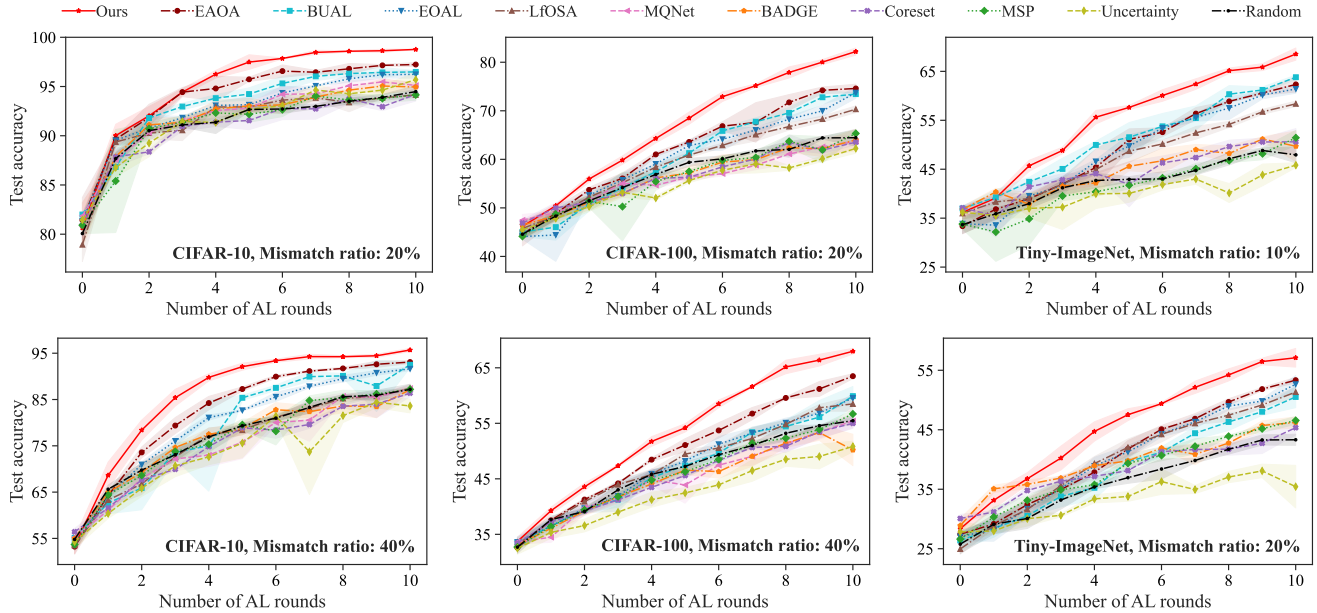


Figure 3. Test accuracy across AL rounds under varying mismatch ratios on CIFAR-10/100 and Tiny-ImageNet.

4. Experiments

Datasets. We evaluate our method E^2OAL on three standard image classification benchmarks: CIFAR-10 [14], CIFAR-100 [14], and Tiny-ImageNet [39], which contain 10, 100, and 200 classes, respectively. To simulate open-set active learning (OSAL) conditions, a subset of classes is designated as “known”, with the remainder treated as “unknown”. The proportion of known classes, referred to as the *mismatch ratio*, is set to 20%, 30%, and 40% for CIFAR-10/100, and 10%, 15%, and 20% for Tiny-ImageNet, introducing varying levels of open-set difficulty.

Training Setup. For each dataset, the labeled pool is initialized by randomly sampling 1% of known-class instances for CIFAR-10 and 8% for CIFAR-100 and Tiny-ImageNet. We perform 10 active learning (AL) rounds, querying 1,500 samples per round. All models adopt a ResNet-50 [9] backbone and are trained with SGD (momentum 0.9, weight decay 5×10^{-4} , batch size 128) for 200 epochs, starting with a learning rate of 0.01 decayed by 0.1 every 60 epochs. Experiments are performed on NVIDIA RTX 3090 GPUs, and all results are averaged over three runs with random seeds $\{1, 2, 3\}$. The target query precision is fixed at $p^* = 0.6$, consistent with prior work [41], while the estimated upper bound of unknown classes is set to $\hat{u}_{max} = 1000$.

Compared Methods. We compare E^2OAL against representative methods from four categories: (1) Random sampling; (2) Informativeness-based approaches, including Uncertainty [18], Coreset [28], and BADGE [2]; (3) Purity-based methods, such as MSP [11] and LfOSA [20]; (4)

Hybrid approaches, including MQNet [21], EOAL [27], BUAL [42], and EAOA [41], which jointly consider informativeness and purity. All methods follow identical training and evaluation protocols for fair comparison.

4.1. Performance Comparison

We assess the classification performance and query effectiveness of E^2OAL on CIFAR-10, CIFAR-100, and Tiny-ImageNet. Figure 3 illustrates the progression of test accuracy across AL rounds, while Figure 4 presents the relationship between mean query precision and mean test accuracy. Due to space constraints, results for intermediate mismatch ratios are provided in Appendix Figures D1 and E1.

As shown in Figures 3 and D1 (Appendix), E^2OAL consistently surpasses all baselines across varying mismatch ratios and datasets, maintaining clear advantages throughout the entire query process. These results demonstrate the robustness and effectiveness of our framework. Among the baselines, hybrid approaches such as EAOA, BUAL, and EOAL outperform single-factor methods by jointly balancing purity and informativeness. However, their reliance on separate detectors and limited use of labeled unknowns restricts overall performance. In contrast, MQNet combines both factors but suffers from inaccurate purity estimation and also fails to effectively leverage labeled unknowns.

Figures 4 and E1 (Appendix) further show that E^2OAL consistently lies in the top-right region, achieving both high query precision and superior test accuracy. Compared with hybrid baselines (e.g., EAOA, BUAL, EOAL), E^2OAL achieves a better balance between precision and in-

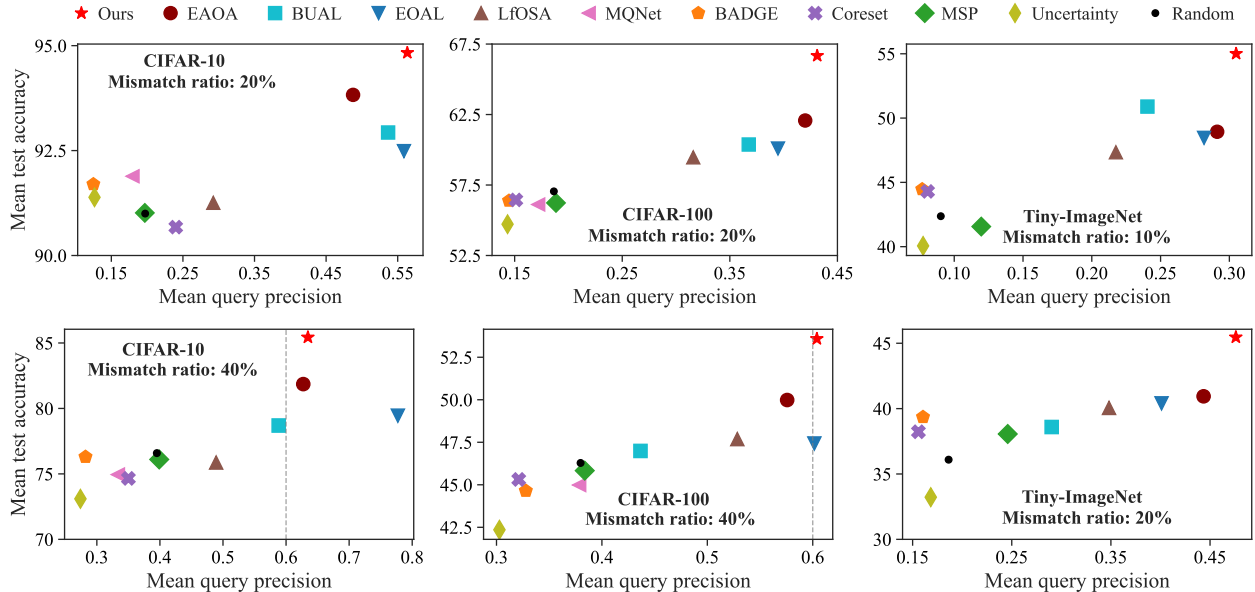


Figure 4. Mean query precision vs. mean test accuracy across rounds under varying mismatch ratios on CIFAR-10/100 and Tiny-ImageNet.

formativeness, attributed to its adaptive sampling and effective use of labeled unknowns. Moreover, E²OAL maintains query precision close to the target $p^* = 0.6$, demonstrating better control than EAOA, which is also guided by a target precision. In contrast, informativeness-only methods (e.g., Uncertainty, Coreset, BADGE) tend to oversample unknowns, while purity-only methods (e.g., MSP, LfOSA) often query redundant known-class samples. By harmonizing these two objectives, E²OAL enables more efficient querying and improved generalization.

In addition, Figure E2 (Appendix) further illustrates how query precision evolves over AL rounds. We observe that even in the early stages, our method consistently maintains high query precision, whereas the previous state-of-the-art method, EAOA, exhibits suboptimal precision and notable fluctuations. This instability originates from the inherent limitation of its adaptive strategy, which updates with a fixed step size and struggles to converge quickly to the optimal value. In contrast, our method introduces no additional hyperparameters and achieves stable, high-precision querying from the outset, demonstrating clear superiority.

4.2. Ablation Studies

Impact of Each Module. We first examine a variant where the target classifier is trained independently without using labeled unknowns, as in prior methods. As shown in Table 1 (see Table F1 in Appendix for complete results), our method still achieves consistent performance gains, particularly on the challenging Tiny-ImageNet, confirming the effectiveness of the proposed adaptive sampling strategy.

We then separately analyze the contributions of the pu-

| Method | CIFAR-10 | CIFAR-100 | Tiny-ImageNet |
|--------|--------------|--------------|---------------|
| Ours* | 95.94 | 67.54 | 60.44 |
| EAOA | 95.88 | 67.14 | 57.31 |
| BUAL | 95.04 | 63.73 | 56.09 |
| EOAL | 93.64 | 63.69 | 56.13 |

Table 1. Final-round test accuracy (%) under fixed mismatch ratios (30% for CIFAR-10/100 and 15% for Tiny-ImageNet). “Ours*” denotes a variant trained without leveraging labeled unknowns.

| Method | CIFAR-10 | CIFAR-100 | Tiny-ImageNet |
|---------------------|-------------|-------------|---------------|
| \mathcal{L}_{EDL} | 9495 | 7934 | 5844 |
| \mathcal{L}_{CE} | 9394 | 7814 | 5661 |

Table 2. Purity comparison under the most challenging mismatch ratios: 20% for CIFAR-10/100 and 10% for Tiny-ImageNet. Sampling by Eq. (6) with CE and EDL losses on the auxiliary head, evaluated by the total number of queried known-class samples.

urity and informativeness components. As presented in Table 2, our Dirichlet-based calibration significantly enhances known-class discrimination, yielding a larger number of known samples among queried instances and thereby improving overall purity. For informativeness, Table 3 shows that our moderately uncertainty-based metric consistently outperforms its counterpart in EAOA—the previous state of the art—achieving higher test accuracy and demonstrating stronger capability in identifying informative samples.

Finally, Table 4 evaluates the contribution of each component. Using only or disabling any single module notably

| Method | CIFAR-10 | CIFAR-100 | Tiny-ImageNet |
|-------------|--------------|--------------|---------------|
| Ours | 95.95 | 65.73 | 48.63 |
| EAOA | 94.90 | 61.95 | 44.73 |
| Uncertainty | 95.37 | 61.28 | 44.73 |

Table 3. Informativeness comparison under the most challenging mismatch ratios: 20% for CIFAR-10/100 and 10% for Tiny-ImageNet. Final test accuracy (%) when retaining only the informativeness component from ‘‘Ours’’, ‘‘EAOA’’, and ‘‘Uncertainty’’.

| Method | CIFAR-10 | CIFAR-100 | Tiny-ImageNet |
|---------------------|--------------|--------------|---------------|
| Ours | 97.52 | 72.10 | 64.02 |
| w/o ClassExp | 97.17 | 70.73 | 62.67 |
| S_{purity} | 96.73 | 72.00 | 61.93 |
| S_{info} | 96.00 | 68.20 | 57.60 |

Table 4. Final-round test accuracy (%) of different ablation variants under intermediate mismatch ratios on CIFAR-10/100 and Tiny-ImageNet. ‘‘ S_{info} ’’ and ‘‘ S_{purity} ’’ denote sampling based solely on informativeness or purity. ‘‘w/o ClassExp’’ disables class expansion by collapsing all labeled unknowns into a single class.

| Mismatch ratio | $p^* = 0.4$ | 0.5 | 0.6 | 0.7 |
|----------------|-------------|--------------|--------------|--------------|
| 20% | 81.47 | 81.67 | 82.20 | 82.18 |
| 30% | 71.90 | 72.96 | 72.10 | 73.17 |
| 40% | 66.68 | 68.03 | 67.98 | 66.78 |

Table 5. Final-round test accuracy (%) on CIFAR-100 under varying target query precisions and mismatch ratios.

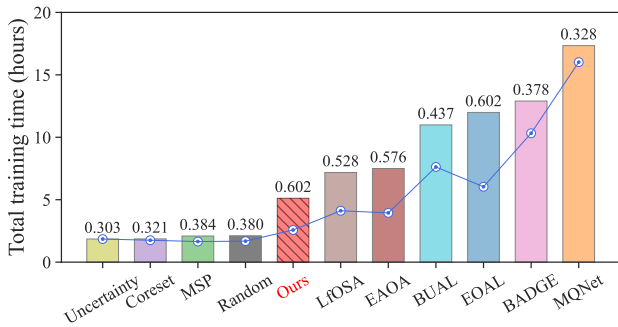


Figure 5. Total training time (hours) on CIFAR-100 under a 40% mismatch ratio. Bars indicate actual training time with the average query precision annotated; the dashed line shows the approximate projection assuming a linear relationship between query precision and time, aligned to the precision level of ‘‘Uncertainty’’.

reduces performance across datasets, confirming that each contributes complementarily to the overall framework.

Sensitivity to Target Precision p^* . In the main experiments, the target query precision p^* is fixed at 0.6, following EAOA. To examine the sensitivity of E²OAL to this param-

eter, we further evaluate it under $p^* \in \{0.4, 0.5, 0.6, 0.7\}$. As shown in Table 5, although the optimal value may vary slightly with the mismatch ratio, E²OAL consistently achieves strong performance across all settings, demonstrating its robustness and adaptability.

Training Efficiency. Figure 5 presents a comparison of the overall and equivalent training times across different methods. E²OAL achieves high training efficiency, with its equivalent time comparable to lightweight baselines such as Random, MSP, Coreset, and Uncertainty. By removing the need for separate detectors and effectively utilizing labeled unknowns, E²OAL attains superior accuracy with only marginal additional cost.

Ablation on \hat{u} Estimation. Figure H1 (Appendix) visualizes how the inferred number of unknown classes \hat{u} evolves across rounds. Even without access to class priors, our adaptive class estimation module exhibits stable convergence and produces estimates that remain within the correct order of magnitude under varying mismatch ratios.

Ablation on Pretrained Representations. Table G1 (Appendix) reports the final-round performance when the default CLIP-extracted features in Algorithm 1 are replaced with representations from a pretrained MoCo [10] backbone. The results show that model accuracy remains largely unchanged, indicating that E²OAL is robust to the choice of pretrained representation. This consistency suggests that the effectiveness of our adaptive estimation strategy primarily arises from the proposed algorithmic design rather than dependence on a specific feature backbone. In practice, CLIP can be substituted with any pretrained model capable of providing high-quality, task-agnostic representations.

5. Conclusion

In this paper, we presented E²OAL, an effective and efficient framework for open-set active learning (OSAL) that reduces wasted annotation cost while significantly improving model performance under open-set conditions. Unlike prior approaches that depend on separate detectors or neglect the value of labeled unknowns, E²OAL leverages them through a two-stage pipeline: (1) an adaptive class estimation and utilization module that uncovers latent structures of labeled unknowns in a frozen semantic space and leverages them to enhance known-class discrimination; and (2) a flexible query strategy that jointly balances informativeness and purity through Dirichlet-based calibration, logit-margin scoring, and a mild uncertainty metric tailored for open-set scenarios. Extensive experiments across multiple OSAL benchmarks demonstrate that E²OAL consistently surpasses prior methods in both accuracy and query effectiveness, while requiring fewer hyperparameters and lower training overhead. Our analysis further highlights the overlooked potential of labeled unknowns as a valuable source of supervisory signal for open-world learning.

Acknowledgements

This work was supported in part by the NSFC (U2441285) and in part by the Interdisciplinary Innovation Fund for Doctoral Students of Nanjing University of Aeronautics and Astronautics.

References

- [1] Sharat Agarwal, Himanshu Arora, Saket Anand, and Chetan Arora. Contextual diversity for active learning. In *European Conference on Computer Vision*, pages 137–153. Springer, 2020. 1
- [2] Jordan T Ash, Chicheng Zhang, Akshay Krishnamurthy, John Langford, and Alekh Agarwal. Deep batch active learning by diverse, uncertain gradient lower bounds. *arXiv preprint arXiv:1906.03671*, 2019. 2, 6, 5
- [3] Maria-Florina Balcan, Andrei Broder, and Tong Zhang. Margin based active learning. In *International Conference on Computational Learning Theory*, pages 35–50. Springer, 2007. 2
- [4] Samuel Budd, Emma C Robinson, and Bernhard Kainz. A survey on active learning and human-in-the-loop deep learning for medical image analysis. *Medical image analysis*, 71: 102062, 2021. 1
- [5] Ting Chen, Simon Kornblith, Mohammad Norouzi, and Geoffrey Hinton. A simple framework for contrastive learning of visual representations. In *International conference on machine learning*, pages 1597–1607. PmlR, 2020. 3
- [6] Pan Du, Suyun Zhao, Hui Chen, Shuwen Chai, Hong Chen, and Cuiping Li. Contrastive coding for active learning under class distribution mismatch. In *Proceedings of the IEEE/CVF International Conference on Computer Vision*, pages 8927–8936, 2021. 1
- [7] Yarin Gal, Riashat Islam, and Zoubin Ghahramani. Deep bayesian active learning with image data. In *International conference on machine learning*, pages 1183–1192. PMLR, 2017. 2
- [8] Julia Grabinski, Paul Gavrikov, Janis Keuper, and Margret Keuper. Robust models are less over-confident. *Advances in neural information processing systems*, 35:39059–39075, 2022. 4
- [9] Kaiming He, Xiangyu Zhang, Shaoqing Ren, and Jian Sun. Deep residual learning for image recognition. In *Proceedings of the IEEE conference on computer vision and pattern recognition*, pages 770–778, 2016. 1, 6
- [10] Kaiming He, Haoqi Fan, Yuxin Wu, Saining Xie, and Ross Girshick. Momentum contrast for unsupervised visual representation learning. In *Proceedings of the IEEE/CVF conference on computer vision and pattern recognition*, pages 9729–9738, 2020. 3, 8
- [11] Dan Hendrycks and Kevin Gimpel. A baseline for detecting misclassified and out-of-distribution examples in neural networks. *arXiv preprint arXiv:1610.02136*, 2016. 6, 1, 5
- [12] Alex Holub, Pietro Perona, and Michael C Burl. Entropy-based active learning for object recognition. In *2008 IEEE Computer Society Conference on Computer Vision and Pattern Recognition Workshops*, pages 1–8. IEEE, 2008. 2
- [13] Sheng-Jun Huang, Rong Jin, and Zhi-Hua Zhou. Active learning by querying informative and representative examples. *Advances in neural information processing systems*, 23, 2010. 1
- [14] A Krizhevsky. Learning multiple layers of features from tiny images. *Master's thesis, University of Tront*, 2009. 6
- [15] Harold W Kuhn. The hungarian method for the assignment problem. *Naval research logistics quarterly*, 2(1-2):83–97, 1955. 4
- [16] Yann LeCun, Yoshua Bengio, and Geoffrey Hinton. Deep learning. *nature*, 521(7553):436–444, 2015. 1
- [17] Changbin Li, Kangshuo Li, Yuzhe Ou, Lance M Kaplan, Audun Jøsang, Jin-Hee Cho, Dong Hyun Jeong, and Feng Chen. Hyper evidential deep learning to quantify composite classification uncertainty. *arXiv preprint arXiv:2404.10980*, 2024. 5
- [18] Mingkun Li and Ishwar K Sethi. Confidence-based active learning. *IEEE transactions on pattern analysis and machine intelligence*, 28(8):1251–1261, 2006. 2, 6, 1, 5
- [19] Hieu T Nguyen and Arnold Smeulders. Active learning using pre-clustering. In *Proceedings of the twenty-first international conference on Machine learning*, page 79, 2004. 2
- [20] Kun-Peng Ning, Xun Zhao, Yu Li, and Sheng-Jun Huang. Active learning for open-set annotation. In *Proceedings of the IEEE/CVF Conference on Computer Vision and Pattern Recognition*, pages 41–49, 2022. 1, 2, 6, 5
- [21] Dongmin Park, Yooju Shin, Jihwan Bang, Youngjun Lee, Hwanjun Song, and Jae-Gil Lee. Meta-query-net: Resolving purity-informativeness dilemma in open-set active learning. *Advances in Neural Information Processing Systems*, 35:31416–31429, 2022. 1, 2, 6, 5
- [22] Fengchao Peng, Chao Wang, Jianzhuang Liu, and Zhen Yang. Active learning for lane detection: A knowledge distillation approach. In *Proceedings of the IEEE/CVF International Conference on Computer Vision*, pages 15152–15161, 2021. 1
- [23] Jon Perez-Cerrolaza, Jaume Abella, Markus Borg, Carlo Donzella, Jesús Cerquides, Francisco J Cazorla, Cristofer Englund, Markus Tauber, George Nikolakopoulos, and Jose Luis Flores. Artificial intelligence for safety-critical systems in industrial and transportation domains: A survey. *ACM Computing Surveys*, 56(7):1–40, 2024. 1
- [24] Haim Permuter, Joseph Francos, and Ian Jermyn. A study of gaussian mixture models of color and texture features for image classification and segmentation. *Pattern recognition*, 39(4):695–706, 2006. 5, 2
- [25] Alec Radford, Jong Wook Kim, Chris Hallacy, Aditya Ramesh, Gabriel Goh, Sandhini Agarwal, Girish Sastry, Amanda Askell, Pamela Mishkin, Jack Clark, et al. Learning transferable visual models from natural language supervision. In *International conference on machine learning*, pages 8748–8763. PmlR, 2021. 1, 3, 4
- [26] Pengzhen Ren, Yun Xiao, Xiaojun Chang, Po-Yao Huang, Zhihui Li, Brij B Gupta, Xiaojiang Chen, and Xin Wang. A survey of deep active learning. *ACM computing surveys (CSUR)*, 54(9):1–40, 2021. 1, 2
- [27] Bardia Safaei, VS Vibashan, Celso M de Melo, and Vishal M Patel. Entropic open-set active learning. In *Proceedings of*

- the AAAI conference on artificial intelligence*, pages 4686–4694, 2024. 1, 2, 6, 5
- [28] Ozan Sener and Silvio Savarese. Active learning for convolutional neural networks: A core-set approach. *arXiv preprint arXiv:1708.00489*, 2017. 1, 2, 6, 5
- [29] Murat Sensoy, Lance Kaplan, and Melih Kandemir. Evidential deep learning to quantify classification uncertainty. *Advances in neural information processing systems*, 31, 2018. 4, 5
- [30] Burr Settles. Active learning literature survey. *Computer Sciences Technical Report 1648, University of Wisconsin–Madison*, 2009. 1, 2
- [31] Manali Sharma and Mustafa Bilgic. Evidence-based uncertainty sampling for active learning. *Data Mining and Knowledge Discovery*, 31(1):164–202, 2017. 1
- [32] Shuzhou Sun, Shuaifeng Zhi, Janne Heikkilä, and Li Liu. Evidential uncertainty and diversity guided active learning for scene graph generation. In *11th International Conference on Learning Representations, ICLR 2023*. OpenReview. net, 2023. 1
- [33] Jiao Tang, Yagao Yue, Peng Wan, Mingliang Wang, Daoqiang Zhang, and Wei Shao. Osal-nd: Open-set active learning for nucleus detection. In *International Conference on Medical Image Computing and Computer-Assisted Intervention*, pages 351–361. Springer, 2024. 1
- [34] Sagar Vaze, Kai Han, Andrea Vedaldi, and Andrew Zisserman. Generalized category discovery. In *Proceedings of the IEEE/CVF conference on computer vision and pattern recognition*, pages 7492–7501, 2022. 4
- [35] Paulo Rafael Soares Oliveira Vieira. Open-world active learning in self-driving cars. Master’s thesis, Universidade de Coimbra (Portugal), 2022. 1
- [36] Yichen Xie, Han Lu, Junchi Yan, Xiaokang Yang, Masayoshi Tomizuka, and Wei Zhan. Active finetuning: Exploiting annotation budget in the pretraining-finetuning paradigm. In *Proceedings of the IEEE/CVF Conference on Computer Vision and Pattern Recognition*, pages 23715–23724, 2023. 1
- [37] Yazhou Yang and Marco Loog. Active learning using uncertainty information. In *2016 23rd International Conference on Pattern Recognition (ICPR)*, pages 2646–2651. IEEE, 2016. 1
- [38] Yang Yang, Yuxuan Zhang, Xin Song, and Yi Xu. Not all out-of-distribution data are harmful to open-set active learning. *Advances in Neural Information Processing Systems*, 36:13802–13818, 2023. 1
- [39] Leon Yao and John Miller. Tiny imagenet classification with convolutional neural networks. *CS 231N*, 2(5):8, 2015. 6
- [40] Donggeun Yoo and In So Kweon. Learning loss for active learning. In *Proceedings of the IEEE/CVF conference on computer vision and pattern recognition*, pages 93–102, 2019. 1
- [41] Chen-Chen Zong and Sheng-Jun Huang. Rethinking epistemic and aleatoric uncertainty for active open-set annotation: An energy-based approach. In *Proceedings of the Computer Vision and Pattern Recognition Conference*, pages 10153–10162, 2025. 1, 2, 6, 5
- [42] Chen-Chen Zong, Ye-Wen Wang, Kun-Peng Ning, Hai-Bo Ye, and Sheng-Jun Huang. Bidirectional uncertainty-based active learning for open-set annotation. In *European Conference on Computer Vision*, pages 127–143. Springer, 2024. 1, 2, 6, 5
- [43] Chen-Chen Zong, Ye-Wen Wang, Ming-Kun Xie, and Sheng-Jun Huang. Dirichlet-based prediction calibration for learning with noisy labels. In *Proceedings of the AAAI Conference on Artificial Intelligence*, pages 17254–17262, 2024. 4, 5

Revisiting Unknowns: Towards Effective and Efficient Open-Set Active Learning

Supplementary Material

A. Full Expression of Equation (4)

The KL divergence term \mathcal{L}_{KL} between the predicted Dirichlet distribution and the uniform prior can be derived as:

$$\begin{aligned}
 \mathcal{L}_{\text{KL}} &= \text{KL}(\text{Dir}(\tilde{\alpha}) \parallel \text{Dir}(\mathbf{1})) \\
 &= \int \text{Dir}(\mathbf{p}; \tilde{\alpha}) \log \frac{\text{Dir}(\mathbf{p}; \tilde{\alpha})}{\text{Dir}(\mathbf{p}; \mathbf{1})} d\mathbf{p} \\
 &= \int \left(\frac{1}{\mathbb{B}(\tilde{\alpha})} \prod_{i=1}^{k+\hat{u}} p_i^{\tilde{\alpha}_i-1} \right) \log \left(\frac{\mathbb{B}(\mathbf{1})}{\mathbb{B}(\tilde{\alpha})} \prod_{i=1}^{k+\hat{u}} p_i^{\tilde{\alpha}_i-1} \right) d\mathbf{p} \\
 &= \log \frac{\mathbb{B}(\mathbf{1})}{\mathbb{B}(\tilde{\alpha})} \int \frac{1}{\mathbb{B}(\tilde{\alpha})} \prod_{i=1}^{k+\hat{u}} p_i^{\tilde{\alpha}_i-1} d\mathbf{p} \\
 &+ \int \left(\log \prod_{i=1}^{k+\hat{u}} p_i^{\tilde{\alpha}_i-1} \right) \left(\frac{1}{\mathbb{B}(\tilde{\alpha})} \prod_{i=1}^{k+\hat{u}} p_i^{\tilde{\alpha}_i-1} \right) d\mathbf{p} \\
 &= \log \frac{\mathbb{B}(\mathbf{1})}{\mathbb{B}(\tilde{\alpha})} + \mathbb{E}_{\mathbf{p} \sim \text{Dir}(\tilde{\alpha})} \left[\log \prod_{i=1}^{k+\hat{u}} p_i^{\tilde{\alpha}_i-1} \right] \\
 &= \log \frac{\mathbb{B}(\mathbf{1})}{\mathbb{B}(\tilde{\alpha})} + \sum_{j=1}^C (\tilde{\alpha}_j - 1) \mathbb{E}_{\mathbf{p}_j \sim \mathcal{B}(\tilde{\alpha}_j, \sum_{i \neq j} \tilde{\alpha}_i)} [\log p_j] \\
 &= \log \left[\frac{\Gamma \left(\sum_{i=1}^{k+\hat{u}} \tilde{\alpha}_i \right)}{\Gamma(k+\hat{u}) \prod_{i=1}^{k+\hat{u}} \Gamma(\tilde{\alpha}_i)} \right] \\
 &+ \sum_{j=1}^{k+\hat{u}} (\tilde{\alpha}_j - 1) \left[\psi(\tilde{\alpha}_j) - \psi \left(\sum_{i=1}^{k+\hat{u}} \tilde{\alpha}_i \right) \right], \tag{9}
 \end{aligned}$$

where $\mathbb{B}(\cdot)$ denotes the multivariate Beta function, $\mathcal{B}(\cdot, \cdot)$ is the standard Beta function, $\Gamma(\cdot)$ represents the Gamma function, and $\psi(\cdot)$ denotes the digamma function. The explicit definitions of $\mathbb{B}(\cdot)$ and $\mathcal{B}(\cdot, \cdot)$ are given by:

$$\mathbb{B}(\tilde{\alpha}) = \frac{\prod_{i=1}^{k+\hat{u}} \Gamma(\tilde{\alpha}_i)}{\Gamma \left(\sum_{i=1}^{k+\hat{u}} \tilde{\alpha}_i \right)}, \tag{10}$$

and

$$\mathcal{B} \left(\tilde{\alpha}_j, \sum_{i \neq j} \tilde{\alpha}_i \right) = \frac{\Gamma(\tilde{\alpha}_j) \Gamma \left(\sum_{i \neq j} \tilde{\alpha}_i \right)}{\Gamma \left(\tilde{\alpha}_j + \sum_{i \neq j} \tilde{\alpha}_i \right)}. \tag{11}$$

B. The Pseudocode of E²OAL

We outline the full workflow of E²OAL in Algorithm B1, which covers each stage of the active learning process.

C. Additional Results for Figure 1

We present additional results over a wider range of mismatch ratios and network architectures beyond those in Figure 1. As illustrated in Figure C1, we evaluate three sampling strategies to assess whether labeled unknowns can enhance known-class learning: (1) random sampling; (2) certainty-based sampling via maximum softmax probability (MSP [11]); and (3) uncertainty-based sampling using the least-confidence criterion [18]. Our observations indicate that, regardless of sampling strategy, mismatch ratio, or network architecture, leveraging fine-grained labels of labeled unknowns within the auxiliary classifier consistently yields the best performance—especially as network capacity increases. Treating all labeled unknowns as a single class typically improves over ignoring them but results in less stable and less substantial gains, occasionally even degrading performance. These findings highlight the significant benefits of effectively exploiting labeled unknowns during training, motivating the in-depth study and method proposed in this work.

D. Additional Results for Figure 3

Figure D1 illustrates the evolution of test accuracy across rounds under intermediate mismatch ratios on three benchmark datasets. E²OAL consistently surpasses all baselines, exhibiting a clearly superior accuracy trajectory throughout the process. Notably, the performance gap widens as the dataset complexity increases, highlighting the robustness and scalability of the proposed framework.

E. Additional Results for Figure 4

Figure E1 reports the mean test accuracy and average query precision across rounds under moderate mismatch ratios on three benchmark datasets. E²OAL achieves the highest query precision on CIFAR-100 and Tiny-ImageNet, while consistently outperforming all competing methods in accuracy. On CIFAR-10, the query precision is slightly lower than EOAL [27], which is expected since our purity control is explicitly regulated by a target precision of 0.6. This observation underscores two key insights: (1) Simply maximizing query purity is not optimal for open-set active learning—although EOAL attains high precision, its queried samples, albeit from known classes, tend to be less informative, leading to suboptimal accuracy; (2) Although E²OAL does not achieve the absolute highest query precision, it adheres more closely to the target value than EAOA [41], which is also guided by the target precision, demonstrating

Algorithm B1 The E²OAL algorithm

Input: Labeled pool $\mathcal{D}_L = \mathcal{D}_L^{kno} \cup \mathcal{D}_L^{unk}$, unlabeled pool \mathcal{D}_U , known class count k , upper limit \hat{u}_{max} , target classifier f_θ , query budget $|\mathcal{B}|$, and target query precision p^* .

Process: (The t -th active learning round)

- 1: **if** $t = 1$ **then**
- 2: # *Model training*
- 3: Train classifier f_θ using \mathcal{L}_{CE} for primary head (k -way) and \mathcal{L}_{EDL} for auxiliary head (k -way)
- 4: # *Purity-based candidate selection*
- 5: Obtain auxiliary head's outputs for all $x \in \mathcal{D}_L \cup \mathcal{D}_U$
- 6: **for** each $x \in \mathcal{D}_L \cup \mathcal{D}_U$ **do**
- 7: Compute purity margin: $S_{\text{purity}}(x) = \max_{c \in \mathcal{C}_k} o_c$
- 8: **end for**
- 9: **else**
- 10: # *Unknown class estimation*
- 11: Estimate \hat{u} based on labeled pool \mathcal{D}_L , known class count k , and upper bound \hat{u}_{max} using Algorithm 1
- 12: # *Model training*
- 13: Train classifier f_θ using \mathcal{L}_{CE} for primary head (k -way) and \mathcal{L}_{EDL} for auxiliary head ($(k + \hat{u})$ -way)
- 14: # *Purity-based candidate selection*
- 15: Obtain auxiliary head's outputs for all $x \in \mathcal{D}_L \cup \mathcal{D}_U$.
- 16: **for** each $x \in \mathcal{D}_L \cup \mathcal{D}_U$ **do**
- 17: Compute purity margin: $S_{\text{purity}}(x) = \max_{c \in \mathcal{C}_k} o_c - \max_{c \in \mathcal{C}_{\hat{u}}} o_c$
- 18: **end for**
- 19: **end if**
- 20: Fit a 3-component Gaussian Mixture Model (GMM) [24] on logit margins $\{S_{\text{purity}}(x)\}$ to model different purity regimes: high (known), low (unknown), and intermediate (ambiguous)
- 21: For each $x \in \mathcal{D}_U$, compute its likelihood under the high-purity component
- 22: Sort \mathcal{D}_U in descending order of the computed likelihoods
- 23: Initialize the candidate pool \mathcal{C}_{pool} with the top $|\mathcal{B}|$ samples from the sorted \mathcal{D}_U
- 24: # *Precision-based candidate refinement*
- 25: Compute the calibrated target query precision $\hat{p}_t^* = \begin{cases} \max(\min(\hat{p}_{t-1}^* + (p^* - \bar{p}_{t-1}^*), 0), 1) & \text{if } t > 1 \\ p^* & \text{if } t = 1 \end{cases}$
- 26: **while** the mean likelihood of the lowest $|\mathcal{B}|$ samples in \mathcal{C}_{pool} is greater than \hat{p}_t^* **do**
- 27: Add the next highest-likelihood sample from \mathcal{D}_U into \mathcal{C}_{pool}
- 28: **end while**
- 29: # *Information-based final query selection*
- 30: **for** each $x \in \mathcal{C}_{pool}$ **do**
- 31: Obtain predicted probability vector \mathbf{p} of x from the primary head
- 32: Let \mathbf{u} be a uniform distribution over all classes
- 33: Let \mathbf{p}^{\max} be a one-hot vector with 1 at $\arg \max(\mathbf{p})$
- 34: Compute information score: $S_{\text{info}}(x) = \text{JS}(\mathbf{p} \parallel \mathbf{u}) \cdot \text{JS}(\mathbf{p} \parallel \mathbf{p}^{\max})$
- 35: **end for**
- 36: Select top $|\mathcal{B}|$ samples from \mathcal{C}_{pool} with the highest $S_{\text{info}}(x)$ scores as the query set \mathcal{B}
- 37: Compute observed query precision: $\bar{p}_t^* = \frac{|\mathcal{B}^{kno}|}{|\mathcal{B}|}$
- 38: Update data pools: $\mathcal{D}_U \leftarrow \mathcal{D}_U \setminus \mathcal{B}$, $\mathcal{D}_L \leftarrow \mathcal{D}_L \cup \mathcal{B}$
- 39: **return** \mathcal{D}_L , \mathcal{D}_U , \bar{p}_t^* , and f_θ for the next round

superior control and stability in purity regulation.

Figure E2 further illustrates how query precision evolves over rounds. It can be observed that our method maintains a high query precision even in the early training stages—a desirable property, as highlighted in [21], where high-purity

samples tend to provide greater utility when the model is still undertrained. This advantage stems from our proposed purity metric and flexible sampling strategy, which effectively constructs high-purity candidate sets. In contrast, the previous state-of-the-art method, EAOA, shows subop-

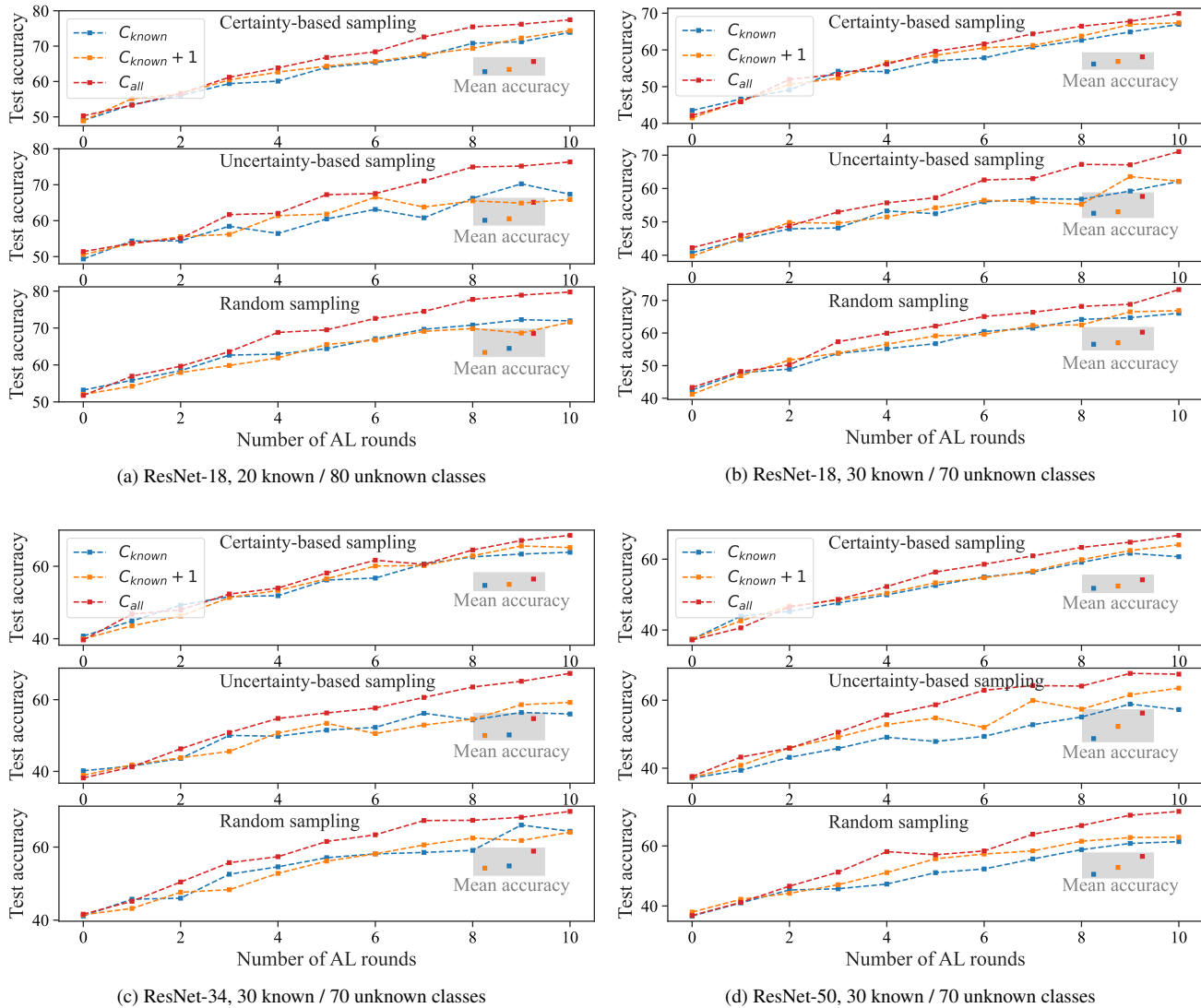


Figure C1. Per-round and mean test accuracy on CIFAR-100 under varying class splits and network architectures. C_{known} excludes labeled unknowns, $C_{known+1}$ collapses them into a single class, and C_{all} leverages their ground-truth labels.

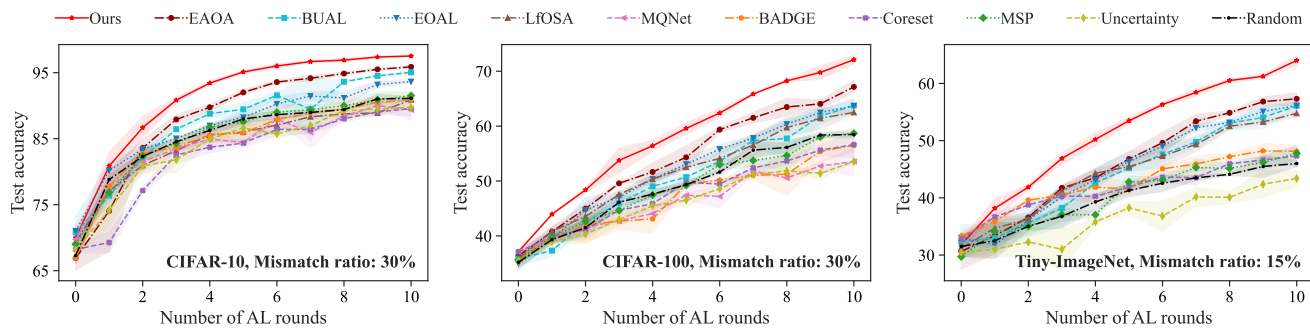


Figure D1. Test accuracy across rounds under mismatch ratio 30% on CIFAR-10/100 and 15% on Tiny-ImageNet.

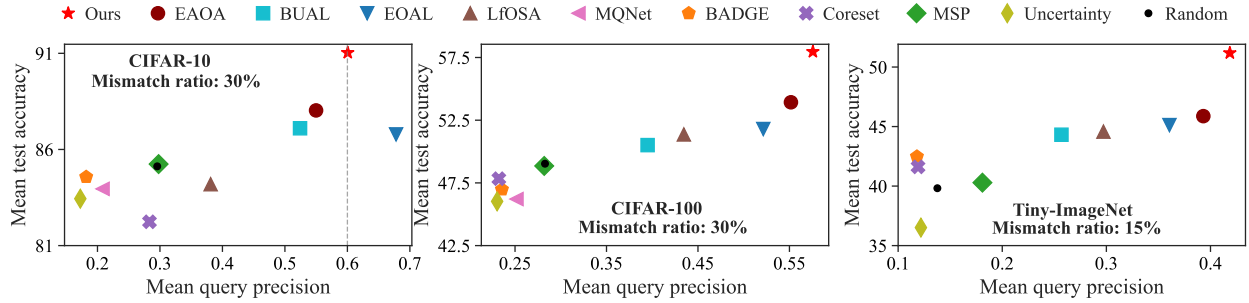


Figure E1. Mean query precision and test accuracy under mismatch ratio 30% on CIFAR-10/100 and 15% on Tiny-ImageNet.

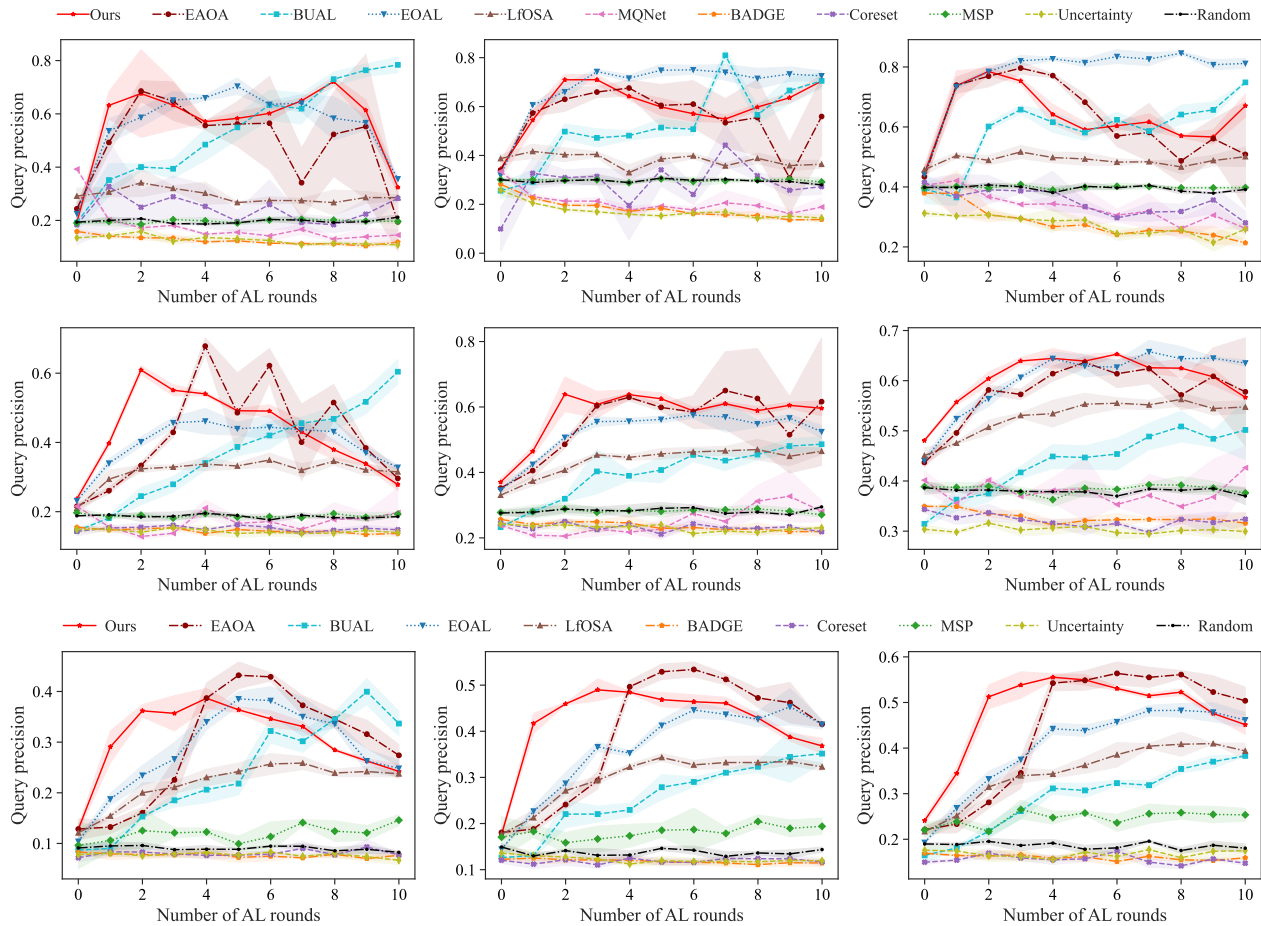


Figure E2. Cross-round query precision under varying mismatch ratios on three benchmarks. From top to bottom: results on CIFAR-10, CIFAR-100, and Tiny-ImageNet; from left to right: mismatch ratios of 20%, 30%, and 40%, respectively.

timal query precision in the early rounds and exhibits significant fluctuations, especially on CIFAR-100 with a 20% mismatch ratio. This instability arises from its inherent limitation in the adaptive sampling strategy, where the adjustment of the parameter k is limited to a fixed step size per round, hindering rapid convergence to an optimal value. Our method, by comparison, introduces no additional hy-

perparameters and achieves stable, high-precision queries from the outset, demonstrating clear superiority.

F. Additional Results for Table 1

Table F1 summarizes the final-round test accuracy of all methods under different mismatch ratios across three

| Dataset | CIFAR-10 | | | CIFAR-100 | | | Tiny-ImageNet | | |
|--------------------------|--------------|--------------|--------------|--------------|--------------|--------------|---------------|--------------|--------------|
| | 20% | 30% | 40% | 20% | 30% | 40% | 10% | 15% | 20% |
| Mismatch ratio | | | | | | | | | |
| Random | 94.48 | 91.11 | 87.18 | 64.45 | 58.48 | 55.48 | 47.93 | 46.00 | 43.32 |
| Uncertainty [18] | 95.70 | 89.77 | 83.61 | 62.25 | 53.52 | 50.83 | 45.83 | 43.40 | 35.43 |
| Coreset [28] | 94.20 | 89.56 | 86.38 | 63.53 | 56.62 | 55.00 | 50.60 | 47.33 | 45.35 |
| BADGE [2] | 94.95 | 90.91 | 87.12 | 64.00 | 56.49 | 50.20 | 49.70 | 48.16 | 46.23 |
| MSP [11] | 94.15 | 91.51 | 87.21 | 65.33 | 58.69 | 56.68 | 51.43 | 47.78 | 46.57 |
| LfOSA [20] | 94.15 | 90.91 | 87.43 | 70.32 | 62.49 | 58.49 | 58.37 | 54.78 | 51.33 |
| MQNet [21] | 95.12 | 89.39 | 87.42 | 63.70 | 53.52 | 55.44 | - | - | - |
| EOAL [27] | 96.23 | 93.64 | 91.63 | 73.73 | 63.69 | 59.55 | 61.40 | 56.13 | 52.65 |
| BUAL [42] | 96.48 | 95.04 | 92.52 | 73.43 | 63.73 | 59.89 | 63.80 | 56.09 | 50.52 |
| EAOA [41] | 97.23 | 95.88 | 93.09 | 74.60 | 67.14 | 63.49 | 62.33 | 57.31 | 53.33 |
| Ours* | <u>97.33</u> | <u>95.94</u> | <u>93.13</u> | <u>75.90</u> | <u>67.54</u> | <u>63.85</u> | <u>64.23</u> | <u>60.44</u> | <u>54.73</u> |
| ↑ over best baseline (%) | 0.10 | 0.06 | 0.04 | 1.30 | 0.40 | 0.36 | 1.15 | 3.13 | 1.40 |
| Ours | 98.77 | 97.52 | 95.69 | 82.20 | 72.10 | 67.98 | 68.53 | 64.02 | 57.10 |
| ↑ over best baseline (%) | 1.44 | 1.64 | 2.60 | 7.60 | 4.96 | 4.49 | 4.73 | 6.71 | 3.77 |

Table F1. Final-round test accuracy (%) of all methods under varying mismatch ratios on CIFAR-10, CIFAR-100, and Tiny-ImageNet. “Ours*” denotes a variant of our method where the target classifier is trained independently without leveraging labeled unknowns. The best result in each setting is highlighted in bold, while the second best is underlined. Due to the poor performance and high training cost of MQNet, we do not include it on Tiny-ImageNet, and thus mark it with “-”.

benchmark datasets. We report results for both “Ours” (the proposed E²OAL) and “Ours*” (a variant where the target classifier is trained independently without utilizing labeled unknowns, similar to prior baselines). Both E²OAL and its variant consistently outperform existing methods by a notable margin. The strong performance of “Ours*” demonstrates the effectiveness of our adaptive sampling strategy in selecting more informative known-class samples, while the additional improvement achieved by E²OAL further highlights the value of leveraging labeled unknowns to enhance known-class learning.

G. Ablation on CLIP Representations

| Feature source | CIFAR-10 | CIFAR-100 | Tiny-ImageNet |
|----------------|--------------|--------------|---------------|
| CLIP | 97.52 | 72.10 | 64.02 |
| MoCo | 97.44 | 72.31 | 63.87 |

Table G1. Final-round test accuracy (%) under fixed mismatch ratios (30% for CIFAR-10/100 and 15% for Tiny-ImageNet). “CLIP” and “MoCo” respectively refer to adaptive class estimation performed using features extracted from a CLIP model and from a self-supervised MoCo pretrained model.

Table G1 presents the final-round results when the default CLIP features are replaced with self-supervised MoCo pretrained representations for adaptive class estimation.

E²OAL exhibits stable performance across all datasets, with only marginal differences between the two feature sources. These results demonstrate that E²OAL is robust to the choice of pretrained representation, and its effectiveness does not depend on a specific feature extractor. In practice, CLIP can be substituted with any pretrained model capable of providing high-quality, task-agnostic features.

H. Ablation on \hat{u} Estimation

Figure H1 illustrates the estimated total number of classes, $k + \hat{u}$, across rounds on CIFAR-100 under mismatch ratios of 20%, 30%, and 40%, where k denotes the number of known classes (20, 30, and 40, respectively). For reference, the figure also includes the final number of queried samples per class. Our adaptive class estimation module consistently yields stable and reliable estimates across rounds and mismatch settings. Since the true class prior of unknown samples is inaccessible, the estimated total number of classes may not exactly match the ground truth. This deviation partly arises from the inherent ambiguity of class granularity—for instance, CIFAR-100 can be organized into either 20 coarse-grained or 100 fine-grained categories. Nevertheless, our method consistently provides estimates within the correct order of magnitude, with accuracy improving as the mismatch ratio increases (i.e., as the open-set problem becomes less challenging). In particular, under the 40% setting, the estimated class count closely fluctuates around the

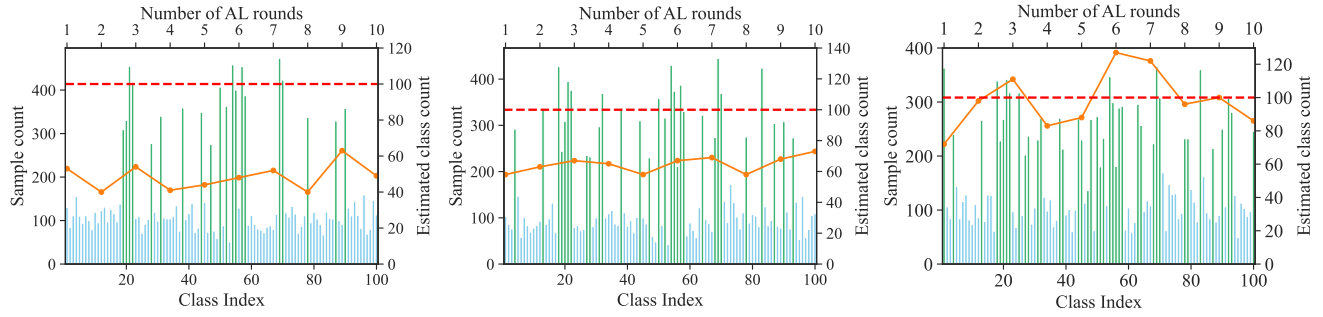


Figure H1. Ablation results for unknown class estimation on CIFAR-100 under mismatch ratios of 20%, 30%, and 40% (from left to right). Bar charts (bottom x-axis and left y-axis) show the total number of samples labeled per class in the final round. Green bars represent known classes, and blue bars represent unknown classes. Line plots (top x-axis and right y-axis) illustrate the evolution of the estimated total number of classes ($k + \hat{u}$), where the ground-truth total is 100.

true value, highlighting the effectiveness and robustness of the proposed class estimation strategy.